Distribution of Dopant Ions Around Poly(3,4-ethylenedioxythiophene) Chains: A Theoretical Study

Jordi Casanovas,[1,*] David Zanuy[2] and Carlos Alemán[2,3,*]

[1] Departament de Química, Escola Politècnica Superior, Universitat de Lleida, c/ Jaume II nº 69, Lleida E-25001, Spain

[2] Departament d'Enginyeria Química, EEBE, Universitat Politècnica de Catalunya, C/ Eduard Maristany, 6-10, 08930, Sant Adriá del Besòs, Spain

[3] Barcelona Research Center for Multiscale Science and Engineering, Universitat Politècnica de Catalunya, Eduard Maristany, 10-14, 08019, Barcelona, Spain

[*] Correspondence to: jcasanovas@quimica.udl.cat and carlos.aleman@upc.edu

ABSTRACT

The effect of counterions and multiple polymer chains on the properties and structure of poly(3,4-ethylenedioxythiophene) (PEDOT) doped with ClO_4^- have been examined using density functional theory (DFT) calculations with periodic boundary conditions (PBC). Calculations on a one-dimensional periodic model with four explicit polymer repeat units and two ClO_4^- molecules indicate that the latters are separated as much as possible, the salt structure and band gap obtained from such ClO_4^- distribution being in excellent agreement with those determined experimentally. On the other hand, DFT calculations on periodic models that include two chains indicate that neighboring PEDOT chains are shifted along the molecular axis by a half of the repeat unit length, dopant ions intercalated between the polymer molecules acting as cement. In order to support these structural features, classical Molecular Dynamics (MD) simulations have been performed on a multiphasic system consisting of 69 explicit PEDOT chains anchored onto a steel surface, explicit ClO_4^- anion embedded in the polymer matrix, and an acetonitrile phase layer onto the polymer matrix. Analyses of the radial distribution functions indicate that the all-*anti* conformation, the relative disposition of adjacent PEDOT chains and the distribution of ClO_4^- dopant ions are fully consistent with periodic DFT predictions. The agreement between such two different methodologies allows reinforce the microscopic understanding of PEDOT films structure.

INTRODUCTION

Conjugated organic polymers (CPs) exhibit an alternated pattern of carbon–carbon single and double bonds lying on the conjugated molecular backbone, which provides a π-orbital overlap along the molecule. These materials have received considerable interest because of their potential applications in technological fields, such as electronics, biomedical engineering, and optics.[1] For example, in the last years they have been proposed for organic batteries,[2,3] biosensors,[4,5] protective coatings for metals,[6,7] electrochromic devices,[8,9] organic light emitting diodes (LEDs),[10] drug delivery sysems[11] and tissue scaffolds.[12,13]

Among the many properties of CPs, the more remarkable are the electrical conductivity and the electrochemical activity (*i.e.* ability to exchange charge reversibly upon oxidation and reduction processes). These advantageous properties are mainly associated to the ability of CPs to undergo fast doping–dedoping processes, combined with their low ionization potential (IP), and low band gap (ε_g).[1,14,15]

Because of the unique characteristics of CPs, a very large number of theoretical works have been conducted to understand structural and environmental effects on their electronic structure. Structural studies concerning neutral and oxidized forms of CPs have shown a distortion from the benzenoid-type structure of the former to the quinoid-type structure on the latter.[16] Thus, the bond length alternation (BLA), which is defined as the difference between the average length of C−C double and single bonds, represents the largest contribution to the ε_g.[17] Consequently, structural modifications on the CPs that leads to a change in the BLA, in turn, can produce a reduction of the π–π^* transition energy.[18]

An extended and generally accepted way to obtain electronic information for CPs is by calculating the properties on oligomers (*i.e.* ignoring chain end effects), plot the

results against inverse chain length and, finally, extrapolate to infinity. Within this well-established strategy the linear extrapolation for oligomers against the reciprocal of the number of repeat units (1/*n*) has been considered as an acceptable procedure to predict the ε_g and IP of CPs. However, experimental results showed that extrapolation fails to consider an asymptotic behavior to derive the electronic properties from the linearization with the inverse of the chain length.[19] Accordingly, different authors proposed that saturation effects should be considered in the extrapolation of such properties with the chain length,[20-22] the different existing approximations being reviewed and compared in a recent study.[23] Another limitation of the approaches based on calculations of finite oligomers is the omission of intermolecular effects. Thus, in addition of intramolecular electronic delocalization, CPs exhibit intermolecular delocalization.[24-29] This contributes to the electron transport from chain to chain in the conduction process. In general, the limitations of calculations on single chain finite oligomers may be overcome by using periodic boundary conditions (PBC).

Another important issue is the influence of the dopant ions that are not covalently bound to the backbone of the CP chains. Experimental results indicate that dopant ions play a crucial role in both the electronic and electrochemical properties of CPs.[1,30-32] Thus, electronic properties depend on the preferred site for the interaction between the dopant ion and the polymer chain while electrochemical activity is related with the mobility of the dopant ions in the polymer matrix. T the number of theoretical studies with dopant ions explicitly taken into account in the calculations is very scarce. These investigations were focused on thiophene[33-38] and pyrrole[39] homo-oligomers, and on periodic polypyrrole,[40] polyaniline,[41] unsubstituted polythiophene[42] and polyacetylene.[43] The latter studies were limited to the parent compounds of the different families of CPs, which are not the most relevant from a technological point of view.

Because of its excellent performance, poly(3,4-ethylenedioxythiophene (PEDOT; Scheme 1) have been settled among the most important CPs.[44-47] PEDOT, which is commercialized under the trade name of Clevios™ (Heraeus) and Baytron® (from H. C. Starck), exhibits low ε_g (1.6-1.7 eV by spectroscopic methods[44] and 1.98 eV by electrochemical measures[48]), easiness to stabilize the oxidized (also named p-doped) state (IP= 4.1-4.3 eV),[48,49] and high conductivity.[44,47] In particular PEDOT films prepared by anodic polymerization in presence of $LiClO_4$ showed excellent electrical conductivity and electrochemical activity.[47,48] Because of these properties, lightweight ClO_4^--doped PEDOT films are frequently used as electrodes for the fabrication of organic electrochemical supercapacitors because of their excellent pseudocapacitance behavior.[50-53] This has been attributed to both (*i*) the redox mechanism, according to which charge is stored by electron transfer from the dopant to the polymer (*i.e.* ion pairing stabilizes the charge); and (*ii*) the double-layer behavior of doped PEDOT chains, which allows resonance throughout the conjugated structure of the polymeric backbone. It is worth noting that dopant···polymer interactions play a crucial role in this energy storage application.

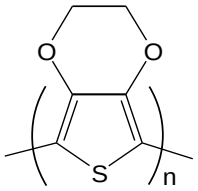

Scheme 1: Chemical structure of PEDOT

In this work we use Density Functional Theory (DFT) calculations to investigate the geometric and electronic structure of PEDOT considering a multi-chain periodic system with explicit ClO_4^- molecules as dopant anions. Furthermore, classical force-field

molecular dynamics (MD) simulations have been carried out on a relatively large model representing the organization of oxidized PEDOT chains grown onto a steel surface by anodic polymerization. In the conducted MD simulations dopant ions embedded in the polymer bulk have been explicitly considered. Results have allowed us to compare the distribution of ClO_4^- derived from small and relatively simple periodic models with that obtained for a more complete description of the polymer matrix.

METHODS

Quantum mechanical calculations. Two different chemical model systems have been examined in this work. The simplest one consists of four 3,4-ethylenedioxythiophene (EDOT) repeat units distributed in a single chain and two ClO_4^- anions, one-dimensional (1D) PBC being applied along the molecular axis (hereafter named *c*-axis). After this, a system containing eight repeat units distributed in two chains doped with two ClO_4^- anions each one, and PBC along the *c*-axis of the unit cell, was considered for calculations. In both cases, different arrangements of the ClO_4^- units with respect to the oligomer chains were investigated. Previous standard ion chromatography[47] and electrochemical[54] studies indicated that the number of positive charges supported by each repeat unit of PEDOT prepared by anodic polymerization in an acetonitrile solution with $LiClO_4$ is +0.5, which is the doping degree set for all the calculations presented in this work.

All DFT calculations were carried out using the Gaussian 09 computer package.[55] Initially, the geometries of the different investigated systems were fully optimized using the B3LYP[56,57] functional combined with the 6-31G(d) basis set and using PBC[58,59] as implemented in Gaussian 09 program. After this, the structures were re-optimized using

the M06L functional,[60] which was developed by Zhao and Truhlar to account for dispersion, combined with the same basis set. No symmetry constraints were used in the geometry optimizations. Calculations were performed considering a null total charge of the systems and singlet state spin restricted wavefunctions. Thus, as each doped PEDOT chain is described by considering four explicit repeat units only, the bipolaron is expected to be the most probable structure. However, in order to corroborate this feature, geometry optimizations on the system with 1D-PBC were also performed considering triplet and singlet states with unrestricted wavefunctions.

The IP of each model system has been determined using the Koopmans' theorem, according to which the IPs have been taken as the negative of the highest occupied molecular orbital (HOMO) energy (*i.e.* $IP^{KT} = -\varepsilon_{HOMO}$). Although Koopman's theorem does not apply to DFT and the energies of Kohn−Sham orbitals do not involve any physical meaning, the Janak's theorem[61] was used by Perdew[62] to show the connection between the IP and the energy of the HOMO. The ε_g was approximated as the difference between the energies of the HOMO and the lowest unoccupied molecular orbital (LUMO) frontier orbitals: $\varepsilon_g = \varepsilon_{LUMO} - \varepsilon_{HOMO}$. In an early work, Levy and Nagy showed that in DFT calculations ε_g can be correctly estimated using this procedure.[63]

Classical Molecular Dynamics Simulations. In our previous experiments, bulk PEDOT was grown over a surface of austenitic stainless steels, or 300 series.[47,48,54] This kind of alloy has a characteristic crystalline structure that consists on a face-centered cubic (fcc) lattice for the iron atom positions, with a cell parameter of 3.65 Å, whereas the minor components are located on punctual interstitial positions that are mostly dependent on the manufacturing company. In order to present a sufficiently reliable representation of the steel structure, whereas avoiding the peculiarities of the minor components, the metallic surface has been modeled as a uniform three-dimensional

organization of 11 layers of frozen iron atoms organized in the fcc lattice. Despite of being a disfavored crystalline organization for the pure metal, the steel electrodes that were experimentally used presented the iron atoms settled in such crystal organization.

A total of 69 PEDOT chains, each one containing 40 repeat units, were constructed and distributed perpendicularly to an iron fcc surface of area 51.1×102.2 $Å^2$. The area of the substrate was selected to fit the experimental density of p-doped PEDOT.[47] Polymer chains were distributed over the surface considering two apparently extreme organizations over such surface. In the first distribution, called HOM, the chains were homogenously and regularly distributed while in the second one, called HET, the chains were randomly distributed. Despite of the heterogeneous location of the chains in HET, the apparition of empty patches in the surface (*i.e.* regions without grown polymer chains) was not produced during the generation process. This was because the density of polymer chains (*i.e.* number of chain per unit of area) was high enough to ensure the lack of empty regions if steric overlaps are avoided if steric overlaps are avoided.

As each repeat unit supports 0.5 positive charge,[47] the number of ClO_4^- ions added to reach charge neutrality was 0.5×40×69 = 1380. Using an strategy envisaged to estimate the unoccupied space of any polymeric solid,[64] the maximum amount of the 1380 ClO_4^- ions were placed in the interstitial zones between polymer chains. The HOM model allowed placing 1356 ClO_4^- ions while the disordered models allowed inserting 1345 ions. The remaining anions were place above the PEDOT layer, separating each ClO_4^- molecule by a minimum radial distance of 5.5 Å to ensure its solvation when the solvent is added. Finally, the HOM and HET models were placed in an orthorhombic cell of 51.1×102.2×240 $Å^3$. All the remaining free space of the simulation box was filled with acetonitrile molecules from a previously equilibrated simulated solvent box that

reproduced the experimental density of this liquid (0.777 $g \cdot cm^{-3}$). The total amount of solvent molecules in the HOM and HET models was 10814.

MD simulations were performed using the NAMD 2.9 program.[65] Each system was submitted to 5000 steps of energy minimization (Newton Raphson method) and this was the starting point of several minicycles of optimization and equilibration. The first equilibration target was the liquid phase, which includes both the solvent and ClO_4^- molecules. This stage was integrated by 80000 steps of heating and equilibration in NVT conditions to thermally stabilize each model at 298K. The Berendesen thermostat was used[66] with a relaxation time of 1 ps, the fast convergence of the external bath was used to improve the efficiency of the thermal equilibration. During such period of time all the solid phase atoms were kept frozen.

Next, the solvent density was equalized to its optimum value using 150000 steps of NPT simulation at 298 K. The Nose–Hoover[67] piston combined with the piston fluctuation control of temperature implemented for Langevin Dynamics[68] was used in this equilibration cycle. Pressure was kept at 1 bar while the oscillation period and the piston decay time were set at 1 ps and 0.001 ps, respectively. The piston temperature was set at the same value as the thermostat control, 298K, which used a damping coefficient of 2 ps. Once the simulation box dimensions were stabilized, the final equilibration cycles were started. After unfreezing all the atoms present in the solid with exception of the iron atoms, 150000 steps of NVT simulation were performed, the Langevin method[69] was used to maintain the system temperature constant with a damping coefficient of 2 ps. Finally, 200000 steps of anisotropic NPT simulation were run to tune each model system to the simulation conditions. For this cycle, the solid surface dimensions were kept by the crystallographic restrictions imposed by the iron structure, and only the *z*-axis dimension was allowed to change. The last snapshot of

this latter run was the starting point of 20 ns of production time. The production runs were performed under the same conditions previously mentioned for the NPT equilibration.

Force-field parameters for PEDOT were extrapolated from AMBER03 libraries[70] with exception of partial charges of the repeat unit, which had previously been parametrized.[71] Acetonitrile molecules were represented by the standard AMBER03 model[70] and ClO_4^- parameters were obtain from Baaden *et al.*[72] AMBER compatible parameters for iron atoms were taken from previous work.[71] The atom pair cut-off distance was set at 14.0 Å to compute the van der Waals interactions. In order to avoid discontinuities in the potential energy function, non-bonding energy terms were forced to slowly converge to zero, by applying a smoothing factor from a distance of 12.0 Å. Beyond cut off distance, electrostatic interactions were calculated by using Particle Mesh of Ewald, with a points grid density of the reciprocal space of 1 $Å^3$.[73] The numerical integration step was set at 1 fs.

RESULTS AND DISCUSSION

1D doped PEDOT model. In order to investigate the preferred locations of the dopant ions, 11 initial arrangements that differ in the relative position of the two ClO_4^- anions with respect to the four explicit polymer repeat units were constructed (Figure 1) and, subsequently, optimized considering 1D-PBC conditions. As it was expected, geometry optimizations of the singlet electronic state using restricted and unrestricted DFT calculations led to identical results, whereas geometries optimized considering a triplet state were unfavored by more than 17 kcal/mol with respect to those calculated in the singlet state. Furthermore, the four structures of lower energy, which are separated by less than 1.5 kcal/mol, exhibited the same distribution of ClO_4^- ions, independently

of the DFT methodology. This corresponds to one anion above the plane containing the thiophene rings while the other is below such plane, as is illustrated in Figure 2a. Obviously, the disposition of the anions at opposite sides of the thiophene rings minimizes the repulsive $ClO_4^- \cdots ClO_4^-$ interactions, favoring an efficient doping process. Furthermore, each anion is directly confronted to the sulfur atom of thiophene ring.

Table 1 compares the electronic properties obtained for periodic models in this work with those reported in previous studies extrapolating from *n*-EDOT oligomers and using the same or similar DFT levels. The ε_g obtained for the four 1D periodic models of lower energy at the B3LYP/6-31G(d) ranges from 1.84 to 2.01 eV. These values are higher than that derived from linear extrapolation to infinite chains considering calculations at the same theoretical level on *n*-EDOT oligomers with *n*= 2-30 (*i.e.* 1.69 eV), whereas they are in good agreement with those obtained using extrapolation methods with saturation effects (*i.e.* 1.75 – 1.94 eV depending on the approach).[23] On the other hand, the IP of the four structures of lower energy obtained for the 1D models varies between 6.42 and 6.51 eV. This interval reflects an overestimation of ~2-3 eV with respect to experimental values[48,49] and theoretical predictions[23] at the similar computational levels (Table 1). We have attributed this overestimation to errors of the exchange-correlation potential in the representation of charge-transfer complexes, which did not influence the linear extrapolation predictions derived from calculations on neutral oligomers.

Results obtained at the M06L/6-31G(d) were very similar to those achieved with the B3LYP functional in terms of distribution of ClO_4^- ions. However, the electronic properties derived from M06L/6-31G(d) calculations were significantly lower than those determined at the B3LYP/6-31G(d) level, as is evidenced in Table 1. Thus, the ε_g

and the IP range from 1.06 to 1.15 eV and from 5.58 to 5.66 eV, respectively. This feature indicates that the M06L functional overestimates the delocalization of π-electrons along the polymer chain.

Analysis of the Mulliken charge distribution pattern (not shown) indicates that each ClO_4^- dopant provokes practically complete transfer of an electron (~0.9 electrons) from the periodic PEDOT backbone, resulting in a divalent salt. Mulliken charges are slightly higher for the thiophene rings located in front of the dopant molecule than for the thiophene located at the center of the explicitly described fragment (*i.e.* ~0.5 against ~0.4 electrons). It is worth noting that this charge distribution is in excellent agreement with the chemical formula experimentally determined for PEDOT doped with ClO_4^-: $[(EDOT^{0.539+})_n(ClO_4^-)_{0.539n}]_{solid}$.[47]

3D doped PEDOT model. The most favored disposition of the dopant ions obtained for the 1D PEDOT model (Figure 2a) was used to construct two different 3D models, which were full optimized considering PBC along the *c*-axis. Both models explicitly contain eight EDOT repeat units distributed in two different chains and four ClO_4^- molecules. In model A the two PEDOT chains adopt an antiparallel disposition, which corresponds to a shift of one repeat unit along the *c*-axis. Depending on the relative disposition of the dopant anions, four different arrangements (Figure 3a) were constructed for model A, hereafter denoted A# (where # varies between 1 and 4). Model B consists of two parallel PEDOT chains, which are translated one with respect to other along one of the axis perpendicular to the *c*-axis (hereafter *b*-axis). Three different arrangement (Figure 3b), labelled as B# (where # ranges from 1 to 3), were considered for this model varying the relative positions of the ClO_4^- molecules. In all initial

arrangements constructed for models A and B, the chlorine atom of each ClO_4^- anion was located in the plane of the closest thiophene ring, in front of the sulfur atom.

Regarding to the results obtained for model A, the most stable arrangement corresponds to A4 (Figure 2b), in which the four explicit ClO_4^- anions are disposed alternatively. Interestingly, the inter-ring dihedral angles (θ) of the PEDOT chains, which are defined by the S–C–C–S sequence, present notable distortions with respect to the ideal *anti* conformation (θ= 180º). More specifically, the three inter-ring dihedral angles of the each explicit polymer chain are [θ= 174.8º, 171.2º and -175.4º] and [θ= -175.3º, -168.8º and 174.8º]. The other three arrangements are destabilized by 3.3 (A1) and more than 20 kcal/mol (A2 and A3). The ε_g and IP calculated for the A4 arrangement is 2.47 and 6.44 eV, respectively. Accordingly, the ε_g increases by ~0.5 eV with respect to the 1D model while the IP remains approximately at the same value, suggesting that the packing of the polymer chains provokes a destabilization of the LUMO. In order to check that such destabilization was not provoked by the loss of planarity, the arrangement A4 was re-optimized fixing all the inter-ring dihedral angles at θ= 180º. The electronic properties of the resulting structure, which was unfavored by 41.8 kcal/mol with respect to the completely optimized one, were ε_g= 2.07 eV and IP= 6.22 eV.

Geometry optimization of the three arrangements constructed for model B (Figure 3b) led to very stable structures. The lowest energy one, which is displayed in Figure 2c, corresponds to the B2 initial conformation. In addition, such structure was found to be favored with respect to the A4 by 2.4 kcal/mol. Analysis of the structure displayed in Figure 2c indicates that the two chains of PEDOT, which in the starting geometry were related by a simple translation vector along the *b*-axis (*i.e.* Δc= 0), undergoes a shift

along the *c*-axis that corresponds to a half of repeat unit. Moreover, the four explicit dopant ions are intercalated between the PEDOT chains, acting as cement between them. On the other hand, the inter-ring dihedral angles of the PEDOT chains obtained for B2, [θ= 176.1º, 179.8º and 176.7º] and [θ= 178.4º, 178.7º and 178.5º], are closer to the ideal *anti* conformation than those obtained for A4.

The ε_g and IP calculated for B2 at the B3LYP/6-31G(d) level is 2.43 and 6.24 eV, respectively, these values being very similar to those obtained for the 1D PEDOT model (Table 1). However, geometry re-optimization of the B2 model at the M06L/6-31G(d) level results in a significant reduction of both ε_g and IP, which reach values of 1.50 and 5.47 eV, respectively. Moreover, the energy gap between the B2 and A4 structures increases 6.7 kcal/mol at the M06L/6-31G(d) level, indicating a strong stabilization of the former disposition with respect to that obtained at the B3LYP/6-31G(d) level. The polymer conformations predicted by the M06L functional for the B2 arrangement, with [θ= 172.3º, 176.5º and 172.5º] and [θ= 178.4º, 174.5º and 178.6º], are similar to those achieved with the B3LYP functional. Similarly, the two functionals predict the same relative positions for the four ClO_4^- anions. However, detailed comparison of the geometries reveals that the two PEDOT chains are ~1 Å closer in the M06L/6-31G(d) geometry than in the B3LYP/6-31G(d) one. This feature is evidenced in Figure 4, which compares the S···S distances for the geometries optimized at the B3LYP/6-31G(d) and M06L/6-31G(d) levels. The M06L exchange-correlation functional improves the description of short and medium range interactions in which correlation plays an important role, as for example π-π stacking,[74,75] while such interactions are neglected by the B3LYP functional. Accordingly, the approximation of the chains at the M06L/6-31G(d) level results in an increment in the electron transport from chain to chain with

respect to the geometry optimized at the B3LYP/6-31G(d) level, which in turn provokes a reduction of the ε_g and the stabilization of the HOMO.

Table 1 provides a complete comparison between the different theoretical and experimental estimates for ε_g and IP. As it can be seen, the B3LYP values derived from extrapolation against 1/*n* and single molecule calculations are in very good agreement with experimental measures. This should be essentially attributed to a cancellation of errors, in which the tendency of the B3LYP functional to overestimate the electronic delocalization along the carbon chain compensates the omission of neighboring polymer chains and explicit dopant molecules. Although this effect is partially maintained in the 1D model studied in this work, it is almost eliminated in the 3D models that involve two explicit polymer chains and dopant anions. More specifically, the electronic properties predicted by the B3LYP functional for the multiple chains models are significantly overestimated. We have attributed this deficiency to the erroneous description of intermolecular electron transport effects, which is probably due to limitations in the exchange-correlation potential for charge-transfer complexes. In contrast, application of the M06L functional to the 3D model reveals a very good agreement with the experimentally determined ε_g (Table 1). Thus, the satisfactory description of dispersion contribution in intermolecular interactions compensates the contribution associated to the delocalization of π-electrons along each molecule, which is overestimated (Table 1). On the other hand, the IP is overestimated by all the periodic models examined in this work, independently of the functional.

Classical MD Simulations. In a recent study we used classical MD simulations to investigate the ultra-structure organization and dynamics of PEDOT deposited by electropolymerization onto a steel surface.[71] Results indicated that the structure of

polymeric films is driven by a subtle balance between the electronic repulsions among positively charged PEDOT chains and the electrostatic attraction among the polymer repeat units and the dopant anions. Independently of the distribution of the polymer chains onto the metallic surface, PEDOT molecules always organized in compact clusters with ClO_4^- anions stabilizing the repeat unit···repeat unit inner electrostatic repulsions by acting as bridging cements. This microstructural organization was found to be fully consistent with the experimental observations, which showed a large number of heterogeneously distributed polymer clusters, each one occupying a relatively small area. Moreover, such molecular description of bulk PEDOT was also in agreement with the electrochemical properties of the material. Thus, the excellent capacity to integrate dopant anions inside the PEDOT matrix is the key factor for its application in supercapacitors.

Despite of such valuable microscopic information, molecular details, as the relative disposition of neighboring polymer chains and the distribution the of the dopant anions with respect to the closest polymer chain, were not examined in our previous study.[71] In this sub-section we investigate such details using a multi-phasic molecular model consisting of 69 explicit PEDOT chains anchored onto a steel surface, 1380 explicit ClO_4^- anion embedded in the polymer matrix and 10814 acetonitrile molecules forming a liquid phase layer onto the polymer matrix (Figure 5). Polymer chains were distributed onto the metallic surface using both homogeneous and heterogeneous distributions (see Methods section).

The relative disposition of the polymer chains has been examined by determining the radial distribution functions (rdf) of the S···S pairs for the thiophene rings of both the HOM and HET models. In order to clarify the interpretation of these results, contributions associated to rings belonging to the same and different polymer chains

have been separated: $g^{\text{intra}}_{\text{S-S, HOM}}(r)$ and $g^{\text{inter}}_{\text{S-S, HET}}(r)$ for the HOM model (Figure 6a) and $g^{\text{intra}}_{\text{S-S, HET}}(r)$ and $g^{\text{inter}}_{\text{S-S, HET}}(r)$ for the HET model (Figure 6b). Analyses of the results derived from DFT calculations on periodic models with two explicit chains reveal that the S···S distances between thiophene rings belonging to the same polymer chain ($d^{\text{intra}}_{\text{S-S}}$) were 4.4, 7.7 and 11.8 Å for both the A4 and B2 models (Figures 2b and 2c, respectively), independently of the functional. The number of values increases significantly when S···S distances between thiophene rings belonging to different chains are considered ($d^{\text{inter}}_{\text{S-S}}$). However, comparison between the B2 and A4 PBC models reveals some unique values, which appear at $d^{\text{inter}}_{\text{S-S}} \approx$ 6.5-6.6 Å and $d^{\text{inter}}_{\text{S-S}} \approx$ 7.0-7.2 Å, respectively.

The $g^{\text{intra}}_{\text{S-S, HOM}}(r)$ and $g^{\text{intra}}_{\text{S-S, HET}}(r)$ profiles (Figure 6a) are practically identical with sharp peaks at 4.3, 7.7, 11.8, 15.5 and 19.5 Å. The perfect match with the three distances measured for DFT periodic models indicate that the inter-ring dihedral angles of the polymer chains rightly adopt an all-*anti* conformation. Early quantum mechanical calculations on unsubstituted 2,2'-bithiophene and its 3,3'-, 4,4'-, and 5,5'-dimethyl derivatives in the neutral state proved that the *anti-gauche* disposition is the preferred when substituents are not fused onto the thiophene rings,[76] the all-anti being only the most stable arrangement in the oxidized state.[77] In contrast, quantum mechanical calculations on 3,4-ethylenedioxythiophene dimer evidenced that the most stable conformation is the fully planar *anti* structure not only in the doped state but also in the neutral one.[78] This was mainly attributed to the restrictions imposed by the fused dioxane ring and to the electron-donating effects provided by the oxygen atoms contained in such cyclic substituent. Results displayed in Figure 6a clearly indicates that the force-field used in this work captures such electronic and geometric effects.

On the other hand, inspection of the $g^{\text{inter}}_{\text{S-S, HOM}}(r)$ and $g^{\text{inter}}_{\text{S-S, HET}}(r)$ profiles (Figure 6b) reveals a broad peak centered at 7.2 Å, whereas no peak is observed around 6.5 Å. This feature indicates that classical MD simulations support the B2 periodic model, which was the one of the lowest energy in DFT calculations, independently of the homogeneous or heterogeneous distribution of the polymer chains onto the metallic surface. The rest of the peaks observed in the two rdf depicted in Figure 6b do not allow an unambiguous differentiation between the A4 and B3 models since they are centered around values close to $d^{\text{inter}}_{\text{S-S}}$ identified in such two DFT models.

The position of the ClO_4^- anions with respect to the polymer chains was derived from the rdf calculated between the centers of masses of the dopant molecule and polymer repeat unit, which have been denoted $g^{\text{HOM}}_{\text{edot-ClO4}}(r)$ and $g^{\text{HET}}_{\text{edot-ClO4}}(r)$ for the HOM and HET models, respectively. As it can be seen in Figure 6c, the profiles of the two models are in excellent agreement, which is consistent with the pair correlation functions displayed in Figures 6a-b. Clear and well-defined peaks appear at 4.2 and 6.0 Å, the latter also showing a shoulder at 7.0 Å. These values exactly match the DFT distances between each ClO_4^- anion and the three surrounding polymer repeat units in the B2 model displayed in Figure 2c (*i.e.* 4.2, 5.9 and 6.9 Å, respectively). Univocal assignment of the other peaks and shoulders displayed in Figure 6c (*i.e.* at 9.5, 10.5 and 12.5 Å) is a difficult task since many of the distances observed in the DFT periodic models are close to such values.

Figure 6d displays the rdf associated to the $ClO_4^- \cdots ClO_4^-$ pairs, which were calculated considering the center of masses of the anions, for the HOM and HET models: $g^{\text{HOM}}_{\text{ClO4-ClO4}}(r)$ and $g^{\text{HET}}_{\text{ClO4-ClO4}}(r)$, respectively. Again there is a good coincidence of the two profiles, indicating that the disposition of the polymer chains

anchored to the metallic surface does not affect significantly the distribution of the ClO_4^- anions. Two well-defined peaks centered at 7.7 and 11.2 Å are observed in the $g^{HOM}_{ClO4\text{-}ClO4}(r)$ profile, these peaks being located at 7.7 and 11.5 Å in the $g^{HET}_{ClO4\text{-}ClO4}(r)$ profile. This is very good agreement with the $ClO_4^- \cdots ClO_4^-$ distances ($d_{ClO4\text{-}ClO4}$) measured for the B2 PBC model, which independently of the functional used for the DFT calculations exhibit four of the six $d_{ClO4\text{-}ClO4}$ values within the interval 7.6-7.8 Å while the other two are 9.8 and 11.7 Å.

The overall of the results derived from classical MD simulations clearly support the structural features of the B2 DFT periodic model. This is an outstanding trend since the size of such DFT model is relatively small. Thus, methodologies based on classical potentials typically provide a good representation of medium- and large-scale properties but a fair, or even very poor, representation of short-scale properties. This limitation is frequently attributed to the following two reasons:[79-82] (1) classical force-fields are not accurate enough to reproduce complex short-range interactions that are essentially controlled by electronic effects; and (2) although classical methodologies enables to consider a large number of explicit particles, calculations on multiphasic systems remain a problem because of the combination of parameters taken from very different sources. However, the electrostatic nature of the short-range interactions in bulk PEDOT and the reliability of the force-field used to describe the metallic substrate, the polymer matrix and the solvent layer of the simulated system have indicated that many structural properties of doped PEDOT (*i.e.* those that are not related with electronic transitions, as for example the benzenoid-to-quinoid transition associated to the own doping process) can be investigated by classical methodologies using a realistic model like that employed in this work. Figure 7 displays a representative picture of such

classical model, in which the similitude with the B2 arranged predicted by periodic DFT calculations is clearly reflected.

CONCLUSIONS

DFT calculations on 1D periodic models of doped PEDOT indicate that the dopant ions are located at opposite sides of the polymer molecules and as far apart as possible, independently of the functional. Both the salt structure and ε_g values obtained with these models are in excellent agreement with experimental data when the B3LYP functional is used, whereas the M06L functional overestimates the electronic delocalization along the polymer chain. Calculations on 3D models with periodic conditions along the molecular axis indicate that the most stable structure corresponds to that in which the two explicit PEDOT chains are shifted a half of repeat unit along the *c*-axis. In this structure the dopant ions are intercalated between the polymer molecules promoting their cohesion. The ε_g is overestimated by the B3LYP functional, which has been attributed to poor representation of PEDOT···PEDOT interactions and, therefore, of intermolecular electron transport effects. In opposition, the ε_g provided by the M06L functional is in good concordance with the available experimental information. However, comparison between the M06L results obtained for 1D and 3D models suggests that such agreement may be due to a compensation of errors.

Classical MD simulations have been used to support the conclusions reached from periodic DFT calculations related to both the distribution of ClO_4^- dopant anions around PEDOT chains and the structural features of the latter. Although methodologies based on force-field potentials do not take into account electronic effects, they provide a reliable description of the electrostatic interactions and, in addition, enable consider multiphasic realistic systems. Results derived from MD simulations considering a large

number of PEDOT chains anchored onto a steel surface and covered with an organic solvent layer are fully consistent with quantum mechanical predictions. Thus, MD simulations reproduce not only basic structural trends, as for example the all-*anti* conformation of PEDOT chains, but also the relative disposition of adjacent polymer chains as well the distribution of dopant agents.

ACKNOWLEDGEMENTS

Authors acknowledge MINECO-FEDER (MAT2015-69367-R) for financial support. Support for the research of C.A. was received through the prize "ICREA Academia" for excellence in research funded by the Generalitat de Catalunya. Authors are indebted to CSUC for computer facilities.

REFERENCES

(1) T. A. Skotheim, R. L. Elsenbaumer and J. R. Reynolds, *Handbook of Conducting Polymers*; Marcel Dekker: New York, 1998.

(2) C. Janaky and K. Rajeshwar, *Prog. Polym. Sci.*, 2016, **43**, 96–135.

(3) S. Ghosh, T. Maiyalagan and R. N. Basu, *Nanoscale*, 2016, **8**, 6921–6947.

(4) G. Yang, K. L. Kampstra and M. R. Abidian, *Adv. Mater.*, 2014, **26**, 4954–4960.

(5) M. Marti, G. Fabregat, F. Estrany, C. Aleman and E. Armelin, *J. Mater. Chem.*, 2010, **20**, 10652–10660.

(6) J. I. Martins, T. C. Reis, M. Bazzaoui, E. A. Bazzaoui and L. I. Martins, *Corros. Sci.*, 2004, 46, 2361–2381.

(7) N. P. Tavandashti, M. Ghorbani, A. Shojaei, J. M. C. Mol, H. Terryn, K. Baert and Y. González-Garcia, *Corr. Sci.*, 2016, **112**, 138–149.

(8) C. W. Hu, T. Kawamoto, H. Tanaka, A. Takahashi, K. M. Lee, S. Y. Kao, Y. C. Liao and K. C. Ho, *J. Mater. Chem. C*, 2016, **4**, 10293–10300.

(9) A. Malti, R. Brooke, X. J. Liu, D. Zhao, P. A. Ersman, M. Fahlman, M. P. Jonsson, M. Bergrren and X. Crispin, *J. Mater. Chem. C*, 2016, **4**, 9680–9686.

(10) C. C. Tang, M. C. Y. Ang, K. K. Cho, V. Keerthi, J. K. Tan, M. N. Syafigah, T. Kugler, J. H. Burroughes, R. Q. Png, L. K. Chua and P. K. H. Ho, *Nature*, 2016, **539**, 536–540.

(11) D. Uppalapati, B. J. Boyd, S. Garg, J. Travas-Sejdic and D. Svirskis, *Biomaterials*, 2016, **111**, 149−162.

(12) A.-D. Bendrea, L. Cianga and I. Cianga, *J. Biomater. Appl.*, 2011, **26**, 3−84.

(13) L. J. Del Valle, D. Aradilla, R. Oliver, F. Sepulcre, A. Gamez, E. Armelin and C. Alemán, *Eur. Polym. J.*, 2007, **43**, 2342−2349.

(14) J. Apperloo, L. B. Groenendaal, H. Verheyen, M. Jayakannan, R. A. Janssen, A. Dkhissi, D. Beljonne, R. Lazzaroni and J. L. Brédas, *Chem. Eur. J.*, 2002, **8**, 2384-2396.

(15) U. Salzner, *J. Chem. Theory Comput.*, 2007, **3**, 1143−1157.

(16) R. Hoffmann, C. Janiak and C. A. Kollmar, *Macromolecules*, 1991, **24**, 3725−3746.

(17) J. Roncali, *Macromol. Rapid Commun.*, 2007, **28**, 1761−1775.

(18) J. Gierschner, J. Cornil and H. J. Egelhaaf, *Adv. Mater.*, 2007, **19**, 173−191.

(19) G. R. Hutchison, Y.-J. Zhao, B. Delley, A. J. Freeman, M. A. Ratner and T. J. Marks, *Phys. Rev. B*, 2003, **68**, 035204.

(20) S. S. Zade and M. Bendikov, *Org. Lett.*, 2006, **8**, 5243−5246.

(21) S. S. Zade and M. Bendikov, *Chem. Eur. J.*, 2008, **14**, 6734−6741.

(22) M. B. Camarada, P. Jaque, F. R: Díaz and M. A. del Valle, *Polym. Sci., Part B: Polym. Phys.*, 2011, **49**, 1723−1733.

(23) J. Torras, J. Casanovas and C. Alemán, C. *J. Phys. Chem. A*, 2012, **116**, 7571−7583.

(24) S. Tsuzuki, K. Honda and R. Azumi, *J. Am. Chem. Soc.*, 2002, **124**, 12200−12209.

(25) L. Miller and K. R. Mann, *Acc. Chem. Res.*, 1996, **29**, 417-423.

(26) V. M. Geskin and J. L. Brédas, *Chem. Phys. Chem.*, 2003, **4**, 498−505.

(27) D. A. Scherlis and N. Marzari, *J. Phys. Chem. B*, 2004, **108**, 17791–17795.

(28) A. Orestis and V. G. Mavrantzas, *Macromolecules*, 2013, **46**, 2450–2467.

(29) H. Liu, S. Kang and J. Y. S.; Lee, *J. Phys. Chem. B*, 2011, **115**, 5113–5120.

(30) W. Chiu, J. Travas-Sejdic, R. Cooney and G. Bowmaker, *Synth. Met.*, 2005, **155**, 80–88.

(31) E. Brillas, K. Carrasco, R. Oliver, F. Estrany and V. Ruiz, V. *Collect. Czech. Chem. Commun.*, 1999, **64**, 1357–1368.

(32) A. D. Bendrea, G. Fabregat, J. Torras, S. Maione, L. Cianga, F. Estrany, L. J. del Valle, I. Cianga and C. Alemán, *J. Mater. Chem. B*, 2013, **1**, 4135–4145.

(33) N. Singh-Miller, D. Scherlis and N. Marzari, *J. Phys. Chem. B*, 2006, **110**, 24822–24826.

(34) C. Alemán, R. Oliver, E. Brillas, J. Casanovas and F. Estrany, *Chem. Phys.*, 2006, **323**, 407-412.

(35) U. Salzner, *J. Chem. Theory Comput.*, 2007, **3**, 1143–1157.

(36) U. Salzner, U. *J. Phys. Chem. A*, 2008, **112**, 5458–5466.

(37) N. Zamoshchik, U. Salzner and M. Bendikov, *J. Phys. Chem. C*, 2008, **112**, 8408–8418.

(38) A. Dkhissi, D. Beljonne and R. Lazzaroni, *Synth. Met.*, 2009, **159**, 546–549.

(39) H. Ullah, A.-H. A. Shah, S. Bilal and K. Ayub, *J. Phys. Chem. C*, 2014, **118**, 17819−17830.

(40) R. Colle and A. Curioni, *J. Am. Chem. Soc.*, 1998, **120**, 4832-4839.

(41) A. Varela-Álvarez, J. Sordo and G. Scuseria, *J. Am. Chem. Soc.*, 2005, **127**, 11318–11327.

(42) N. Zamoshchik and M. Bendikov, *Adv. Funct. Mater.*, 2008, **18**, 3377–3385.

(43) A. Ramirez-Solis, C. Zicovich-Wilson and B. Kirtman, *J. Chem. Phys.*, 2006, **124**, 244703.

(44) L. B. Groenendaal, F. Jonas, D. Freitag, H. Pielartzik and J. R. Reynolds, *Adv. Mater.*, 2000, **12**, 481–494.

(45) S. Kirchmeyer and K. Reuter, K. *J. Mater. Chem.*, 2005, **15**, 2077–2088.

(46) L. Pettersson, T. Johansson, F. Carlsson, H. Arwin and O. Inganas, *Synth. Met.*, 1999, **101**, 198–199.

(47) C. Ocampo, R. Oliver, E. Armelin, C. Alemán, and F. Estrany, *J. Polym. Res.*, 2006, **13**, 193–200.

(48) D. Aradilla, F. Estrany and C. Alemán, *J. Appl. Polym. Sci.*, 2011, **121**, 1982–1991.

(49) C. R. G. Grenier, W. Pisula, T. J. Joncheray, K. Müllen and J. R. Reynolds, *Angew. Chem. Int. Ed.*, 2007, **46**, 714–717.

(50) D. Aradilla, F. Estrany, F. Casellas, J. I. Iribarren and C. Alemán, *Org. Electr.*, 2014, **15**, 40–46.

(51) M. M. Pérez-Madrigal, F. Estrany, E. Armelin, D. D. Díaz and C. Alemán, *J. Mater. Chem. A*, 2016, **4**, 1792–1805.

(52) D. Aradilla, F. Estrany and C. Alemán, *J. Phys. Chem. C*, 2011, **115**, 8430–8438.

(53) M. M. Pérez-Madrigal, M. G. Edo, A. Díaz, J. Puiggalí and C. Alemán, *J. Phys. Chem. C*, 2017, **121**, 3182–3193.

(54) D. Aradilla, D. Azambuja, F. Estrany, M. T. Casas, C. A. Ferreira and Alemán, C. *J. Mater. Chem.*, 2012, **22**, 13110–13122.

(55) Gaussian 09, Revision A.02, M. J. Frisch, G. W. Trucks, H. B. Schlegel, G. E. Scuseria, M. A. Robb, J. R. Cheeseman, G. Scalmani, V. Barone, B. Mennucci, G. A. Petersson, H. Nakatsuji, M. Caricato, X. Li, H. P. Hratchian, A. F. Izmaylov, J. Bloino, G. Zheng, J. L. Sonnenberg, M. Hada, M. Ehara, K. Toyota, R. Fukuda, J. Hasegawa, M. Ishida, T. Nakajima, Y. Honda, O. Kitao, H. Nakai, T. Vreven, J. A. Montgomery Jr, J. E. Peralta, F. Ogliaro, M. Bearpark, J. J. Heyd, E. Brothers, K. N. Kudin, V. N. Staroverov, R. Kobayashi, J. Normand, K. Raghavachari, A. Rendell, J. C. Burant, S. S. Iyengar, J. Tomasi, M. Cossi, N. Rega, J. M. Millam, M. Klene, J. E. Knox, J. B. Cross,

V. Bakken, C. Adamo, J. Jaramillo, R. Gomperts, R. E. Stratmann, O. Yazyev, A. J. Austin, R. Cammi, C. Pomelli, J. W. Ochterski, R. L. Martin, K. Morokuma, V. G. Zakrzewski, G. A. Voth, P. Salvador, J. J. Dannenberg, S. Dapprich, A. D. Daniels, O. Farkas, J. B. Foresman, J. V. Ortiz, J. Cioslowski and D. J. Fox, Gaussian, Inc., Wallingford, CT, 2009.

(56) C. Lee, W. Yang and R. G. Parr, *Phys. Rev. B*, 1988, **37**, 785–789.

(57) A. D. Becke, *J. Chem. Phys.*, 1993, **98**, 5648–652.

(58) K. Kudin and G. E. Scuseria, *Chem. Phys. Lett.*, 1998, **289**, 611–616.

(59) K. Kudin and G. E. Scuseria, *Phys. Rev. B*, 2000, **61**, 16440–16453.

(60) Y. Zhao and D. G. Truhlar, *Theor. Chem. Acc.*, 2008, **120**, 215–241.

(61) J. F. Janak, *Phys. Rev. B*, 1978, **18**, 7165–7168.

(62) J. P. Perdew, In *Density Functional Methods in Physics*; Dreizler, R. M., Providenca, J., Eds.; Plenum Press: New York and London, 1985.

(63) M. Levy and A. Nagy, *Phys. Rev. A*, 1999, **59**, 1687–1689.

(64) D. Curcó, D. Zanuy, and C. Aleman, *J. Comput Chem*., 2003, **24**, 1208–1214.

(65) J. C. Phillips, R. Braun, W. Wang, J. Gumbart, E. Tajkhorshid, E. Villa, C. Chipot, R. D. Skeel, L. Kale and K. Schulten, *J. Comput. Chem.*, 2005, **26**, 1781–1802.

(66) H. J. C. Berendsen, J. P. M. Postma, W. F. van Gunsteren, A. DiNola and J. R. Haak, *J. Chem. Phys.*, 1984, **81**, 3684–3690.

(67) G. J. Martyna, D. L. Tobias and M. L. Klein, M.L. *J. Chem. Phys*., 1994, **101**, 4177–4189.

(68) S. E. Feller, Y. Zhang, R. W. Pastor and B. R. Brooks, *J. Chem. Phys.*, 1995, **103**, 4613–4622.

(69) S. Toxvaerd, *J. Chem. Phys.*, 1990, **93**, 4290–4295.

(70) Y. Duan, C. Wu, S. Chowdhury, M. C. Lee, G. Xiong, W. Zhang, R. Yang, P. Cieplak, R. Luo, T. Lee, J. Caldwell, J. Wang and P. A. Kollman, *J. Comput. Chem.*, 2003, **24,** 1999–2012.

(71) D. Zanuy and C. Alemán, *Soft Matter*, 2013, **9**, 11634–11644

(72) M. Baaden, M. Burgard, C. Boehme and G. Wipff, *Phys. Chem. Chem. Phys.*, 2001 , **3**, 1317–1322.

(73) A. Toukmaji, C. Sagui, J. Board and T. Darden, *J. Chem. Phys.*, 2000, **113**, 10913–10927.

(74) Y. Zhao and D. G. Truhlar, *Acc. Chem. Res*, 2008, **41**, 157–167.

(75) K. Remya and C. H. Suresh, *J. Comput. Chem.*, 2013, **34**, 1341–1353.

(76) C. Alemán and L. Julia, *J. Phys. Chem.*, 1996**, 100**, 1524–1529.

(77) C. Alemán and J. Julia, *J. Phys. Chem.*, 1996**, 100**, 14661–14664.

(78) J. Poater, J. Casanovas, M. Solà and C. Alemán, *J. Phys. Chem. A*, 2010**,** 114, 1023–1028.

(79) R. B. Best, N.-V. Buchete and G. Hummer, *Biophys. J.*, 2008, **95**, 4494–4494.

(80) K. Lindorff-Larsen, P. Maragakis, S. Piana, M. P. Eastwood, R. O. Dror and D. E. Shaw, *Plos One*, 2012, **7**, e32131.

(81) D. Petrov and B. Zagrovic, *Plos Comput. Biol.*, 2014, **10**, e1003638.

CAPTIONS TO FIGURES

Figure 1. Initial disposition of the ClO_4^- anions in doped PEDOT considered for 1D PBC calculations. The empty circle indicates that the ClO_4^- anion is located in the same plane that the thiophene rings while grey and black circles refer to ClO_4^- anions above and below the plane of the thiophene rings, respectively. Double bonds in the PEDOT repeat units are not indicated.

Figure 2. (a) Top and side views of the most favored distribution of the ClO_4^- anions in doped PEDOT as derived from 1D PBC calculations. (b-c) Lowest energy arrangement obtained for models (b) A and (c) B. Three orthogonal projections are displayed for each structure. The lowest energy structure of model B, denoted B2, is 2.4 kcal/mol more stable than the lowest energy structure of model A, denoted A4. The atoms explicitly included in the unit cell corresponds to those depicted using a ball and stick model while atoms represented using a thin stick model correspond to periodic images.

Figure 3. Initial disposition of the ClO_4^- anions and polymer chains in 3D doped PEDOT models considered for PBC calculations: (a) Model A, in which the two PEDOT are shifted by one repeat unit (antiparallel disposition), was constructed considering four different relative arrangements of the ClO_4^- anions; and (b) Model B, in which the two PEDOT are simply translated along an axis perpendicular to the molecular axis (parallel disposition), was constructed considering three different relative arrangements of the ClO_4^- molecules. In all cases the chlorine atom of the dopant molecules was located in the plane of the closest thiophene ring, in front of the sulfur atom.

Figure 4. Top view of the lowest energy 3D model of PEDOT derived from geometry optimization at the (a) B3LYP/6-31G(d) and (b) M06L/6-31G(d) levels. In both cases, the lowest energy model corresponds to the B2 arrangement. The S···S distances are displayed for comparison.

Figure 5. Simulation box used for the MD simulations of the HOM and HET models of bulk PEDOT deposited onto a metallic surface. The multiphase nature of the used molecular model is explicitly depicted.

Figure 6 Radial distribution functions for the HOM and HET models: (a) S···S pairs of thiophene rings located at the same polymer chain; (b) S···S pairs of thiophene rings located at different polymer chains; (c) repeat unit$\cdots ClO_4^-$ pairs; and (d) ClO_4^- $\cdots ClO_4^-$ pairs. Profiles (c) and (d) were calculated using the center of masses of the polymer repeat units and ClO_4^- anions.

Figure 7. Amplified image depicting a representative region of the multiphasic system simulated by classical MD.

Table 1. Band gap (ε_g; in eV) and ionization potential (IP; in eV) of doped PEDOT predicted from periodic and extrapolation models using DFT calculations. Experimental values have been included for comparison.

Model	ε_g (reference)	IP (reference)
1D PEDOT-PBC (4 structures with $\Delta E < 1.5$ kcal/mol)	1.84-2.01[a], 1.06-1.15[b]	6.42-6.51[a], 5.58-5.66[b]
3D PEDOT-PBC (model A4)	2.47[a]	6.44[a]
3D PEDOT-PBC (model B2)	2.43[a], 1.50[b]	6.24[a], 5.47[b]
n-EDOT (*n*= 2-30) - linear extrapolation	1.69 (23)[a]	-
n-EDOT (*n*= 2-8) - linear extrapolation	1.66 (23)[a]	3.71[c] (23)
n-EDOT (*n*= 2-30) - extrapolation with saturation effects	1.75-1.94 (23)[a]	3.55[d], 3.87[e] (23)
Experimental	1.6-1.7 (44),[f] 1.98 (48)[g]	4.1-4.3 (48,49)[g]

[a] Calculated at the B3LYP/6-31G(d) level. [d] Calculated at the M06L/6-31G(d) level. [c] Calculated at the B3PW91/6-31+G(d,p) level. [d] Vertical IP. [e] Adiabatic IP. [f] UV-vis spectroscopy. [g] Cyclic voltammetry.

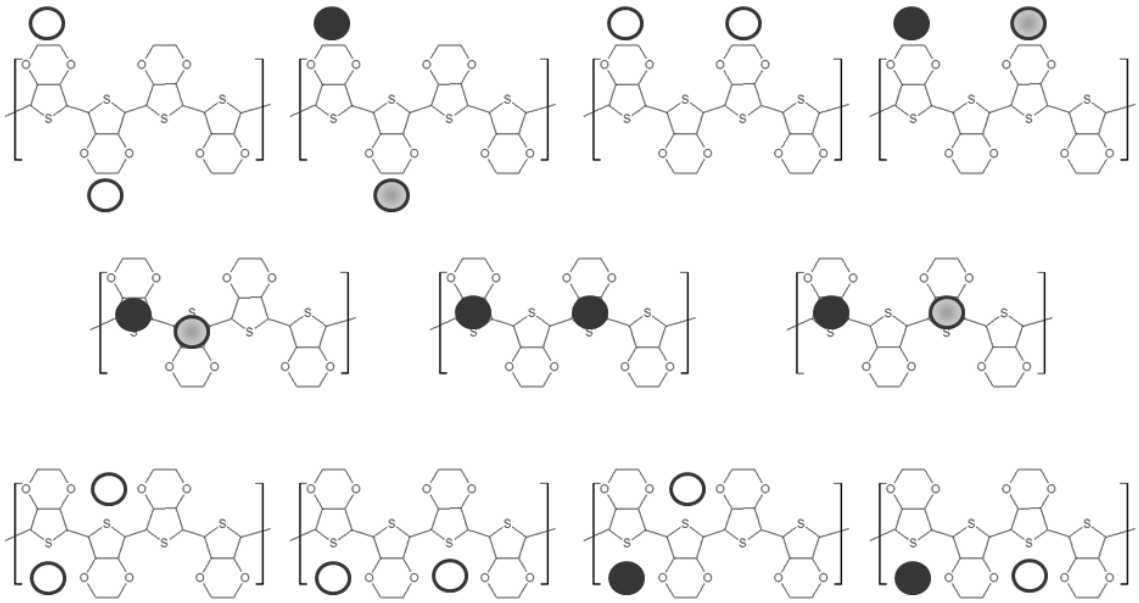

Figure 1

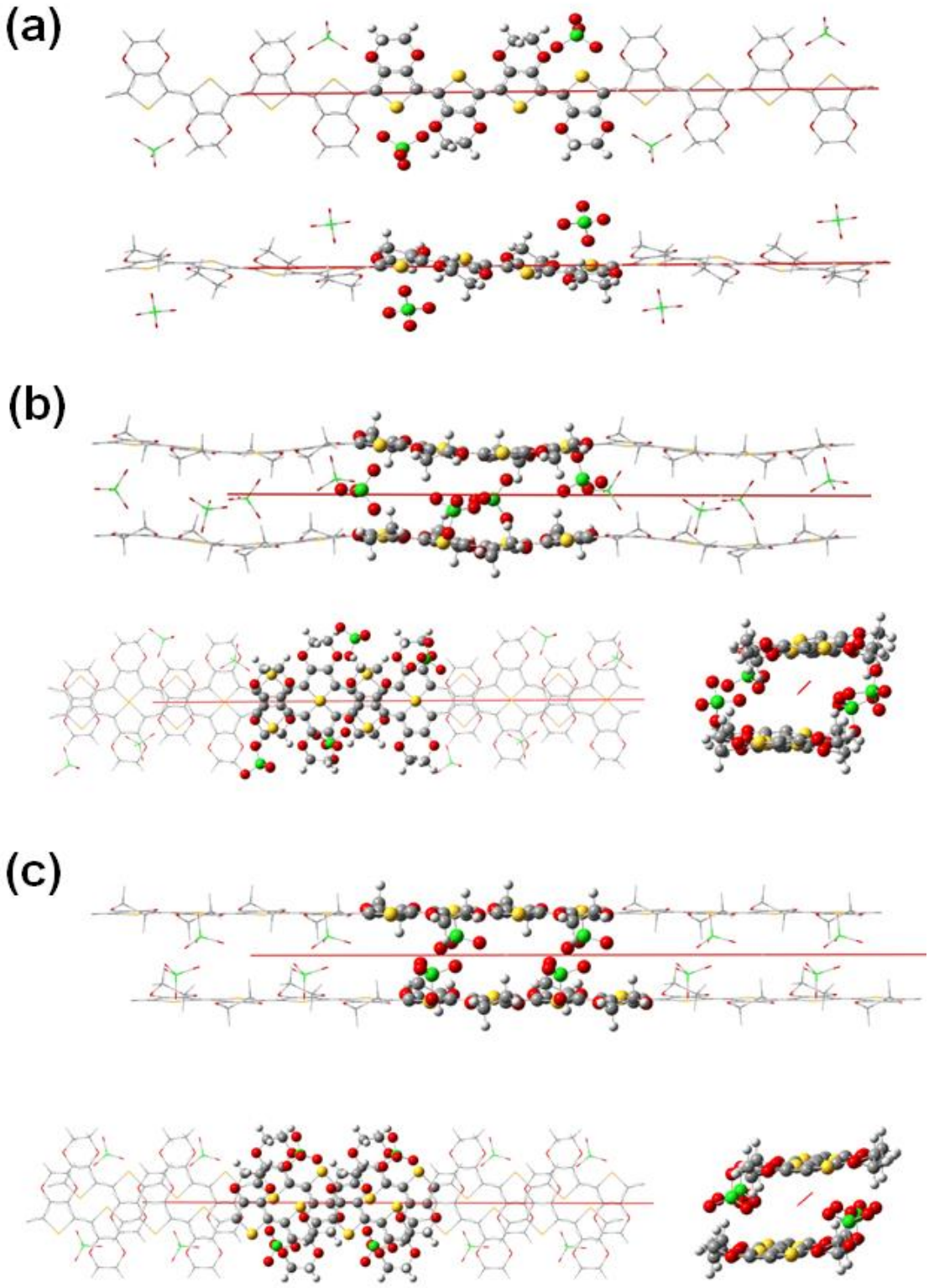

Figure 2

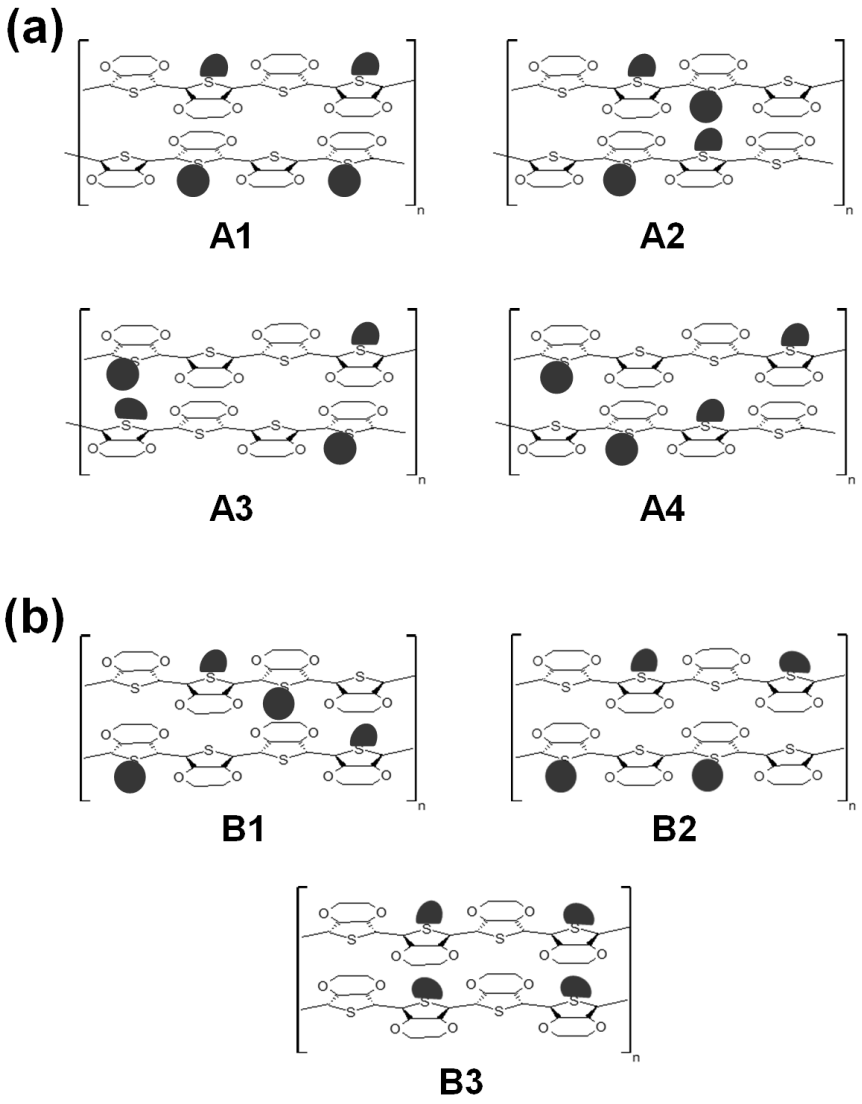

Figure 3

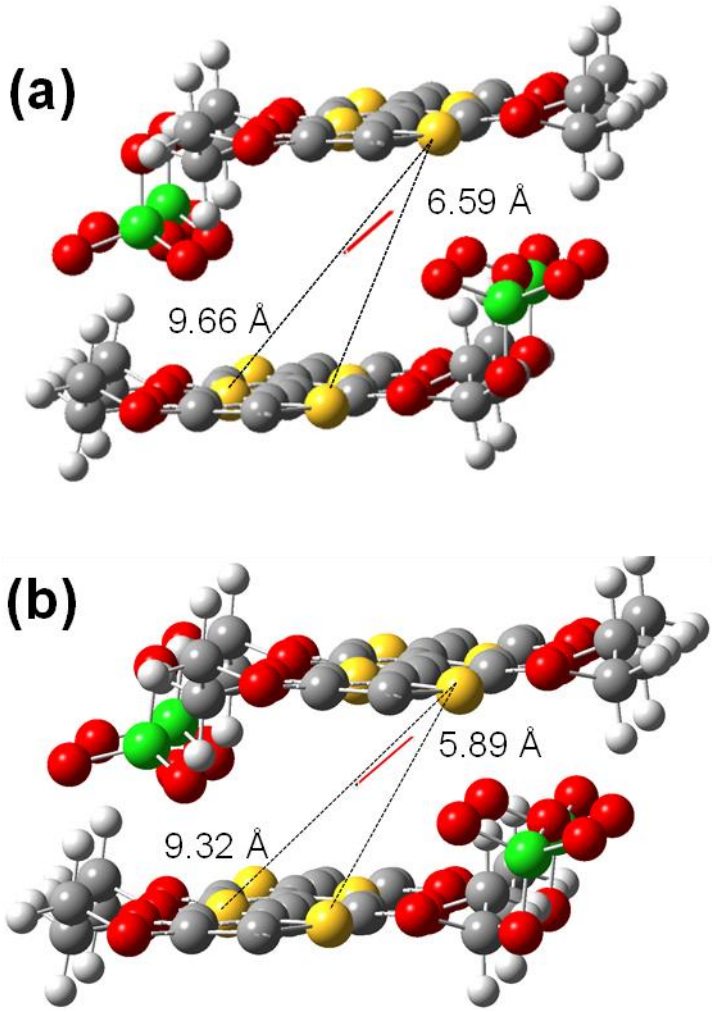

Figure 4

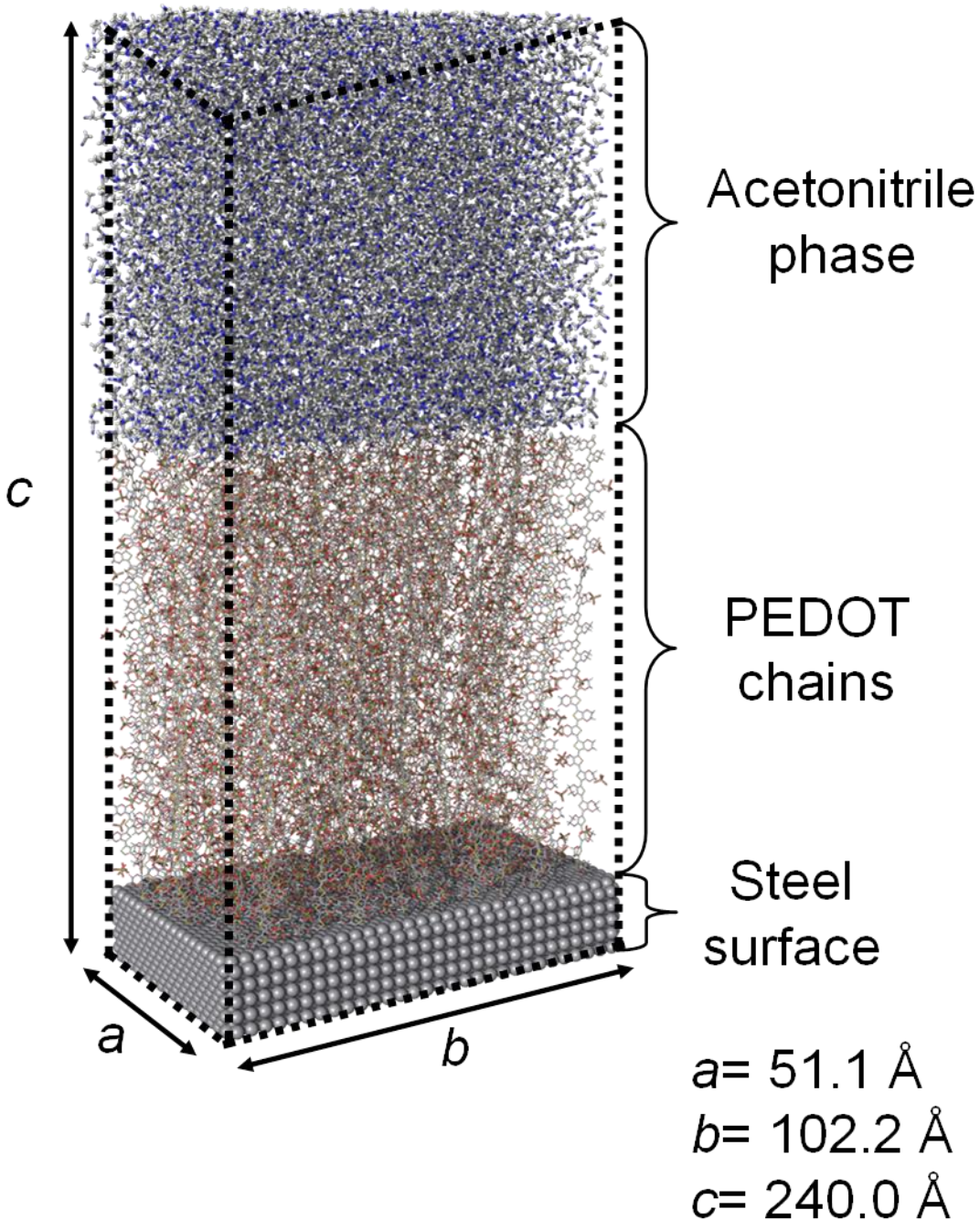
c
Acetonitrile phase
PEDOT chains
Steel surface
a
b
a= 51.1 Å
b= 102.2 Å
c= 240.0 Å

Figure 5

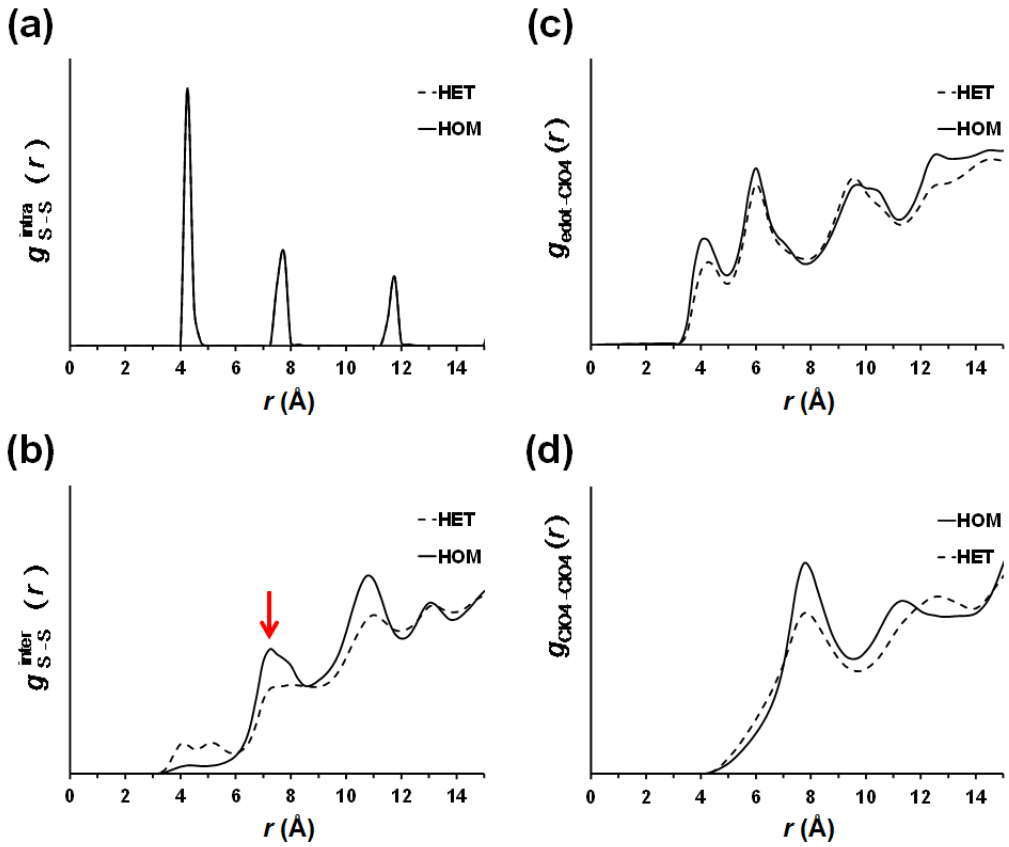

Figure 6

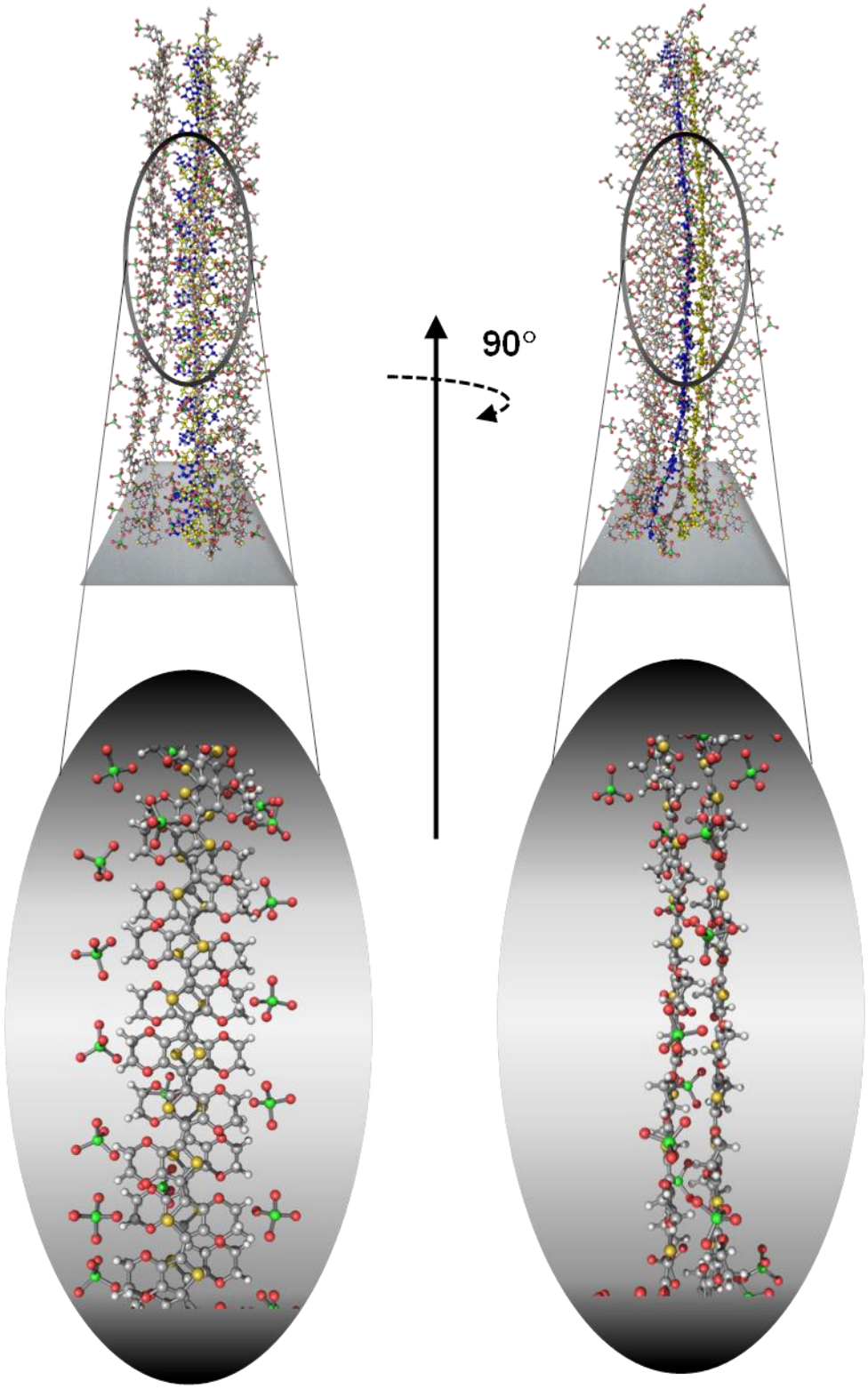

Figure 7

GRAPHICAL ABSTRACT